

MoS₂ Tribotronic Transistor for Smart Tactile Switch

Fei Xue, Libo Chen, Longfei Wang, Yaokun Pang, Jian Chen, Chi Zhang,*
and Zhong Lin Wang*

A novel tribotronic transistor has been developed by vertically coupling a single-electrode mode triboelectric nanogenerator and a MoS₂ field effect transistor. Once an external material contacts with or separates from the device, negative charges are induced by triboelectrification on the surface of the polymer frictional layer, which act as a “gate” voltage to modulate the carrier transport in the MoS₂ channel instead of the conventional applied gate voltage; the drain-source current can be tuned in the range of 1.56–15.74 μ A, for nearly ten times. The application of this MoS₂ tribotronic transistor for the active smart tactile switch is also demonstrated, in which the on/off ratio can reach as high as ≈ 16 when a finger touches the device and the increased drain-source current is sufficient to light two light-emitting diodes. This work may provide a technique route to utilize the 2D materials based tribotronic transistors in micro-electromechanical systems (MEMS), nanorobotics, and human–machine interfacing.

force sensors based on MoS₂ FETs is of great interest. In order to sense externally applied mechanical stimulus, those FETs usually need to be integrated with a piezoelectric layer, in which the drain-source current is tuned by the potential created by piezoelectric polarization charges.^[15,16]

Since 2012, triboelectric nanogenerator has been successfully developed for converting mechanical energy into electricity and as self-powered active mechanical sensors.^[17–22] Based on this new unprecedented energy conversion technology, an interesting field of tribotronics is recently proposed, which states that the electrostatic potential created by triboelectrification between two materials can act as a “gate” voltage to tune the carrier transport in the transistor.^[23] This tribotronic effect

has been reported to offer an innovative and effective method to apply silicon-based and organic FETs in human–machine interfacing.^[24–27]

Here we demonstrate a novel tribotronic transistor based on the vertically coupling of a triboelectric nanogenerator in single electrode mode (S-TENG) and a MoS₂ FET for the first time. A polytetrafluoroethylene (PTFE) film was smoothly attached on the back gate of the as-fabricated MoS₂ transistor to serve as a friction layer. Once an external aluminum layer contacts with or separates from the PTFE film, the drain-source current is dramatically modulated by the triboelectric charges produced on the surfaces of the two materials. Furthermore, when a finger touch is applied on or release from the PTFE film, this MoS₂ tribotronic device can be used as an active smart tactile switch with striking on/off characteristics. This work may provide a technology route to utilize the 2D materials based tribotronic transistors in the fields of MEMS, nanorobotics, and active flexible electronics.

1. Introduction

Molybdenum disulfide (MoS₂), owing to its superior electrical, optical, and piezoelectric properties, is emerging as an excellent 2D material for future electronics.^[1–10] Each MoS₂ layer is constructed by a molybdenum atoms plane sandwiched between two planes of sulfur atoms, with the covalently bonded S–Mo–S atoms in a hexagonal structured crystal. Monolayer or few-layer MoS₂ has been confirmed to possess a band-gap of 1.85–1.2 eV.^[11–13] When integrated with an ideal dielectric layer, a series of field effect transistors (FETs) based on this 2D semiconducting material is demonstrated with high mobility and on/off ratio, near-ideal sub-threshold swing, and large current saturation window.^[1,14] As motivated by the urgent needs for advanced artificial intelligence and human–machine interfacing, the development of low-cost and sensitive strain/

F. Xue, L. Chen, L. Wang, Y. Pang,
J. Chen, Prof. C. Zhang, Prof. Z. L. Wang
Beijing Institute of Nanoenergy and Nanosystems
Chinese Academy of Sciences
National Center for Nanoscience and Technology
(NCNST)
Beijing 100083, P. R. China
E-mail: czhang@binn.cas.cn;
zhong.wang@mse.gatech.edu
Prof. Z. L. Wang
School of Material Science and Engineering
Georgia Institute of Technology
Atlanta, GA 30332, USA



DOI: 10.1002/adfm.201504485

2. Principle and Characteristics

2.1. Structure of the MoS₂ Tribotronic Transistor

Single or few-layer MoS₂ flake was obtained from bulk MoS₂ through the mechanical exfoliation method and directly transferred to the highly doped p-type silicon substrate with 300 nm thick SiO₂ for preparing the MoS₂ tribotronic transistor, as shown in **Figure 1a**, in which the semiconducting MoS₂ is three layers, and the corresponding side-view of atom stacking is shown in the right-hand inset. The source and

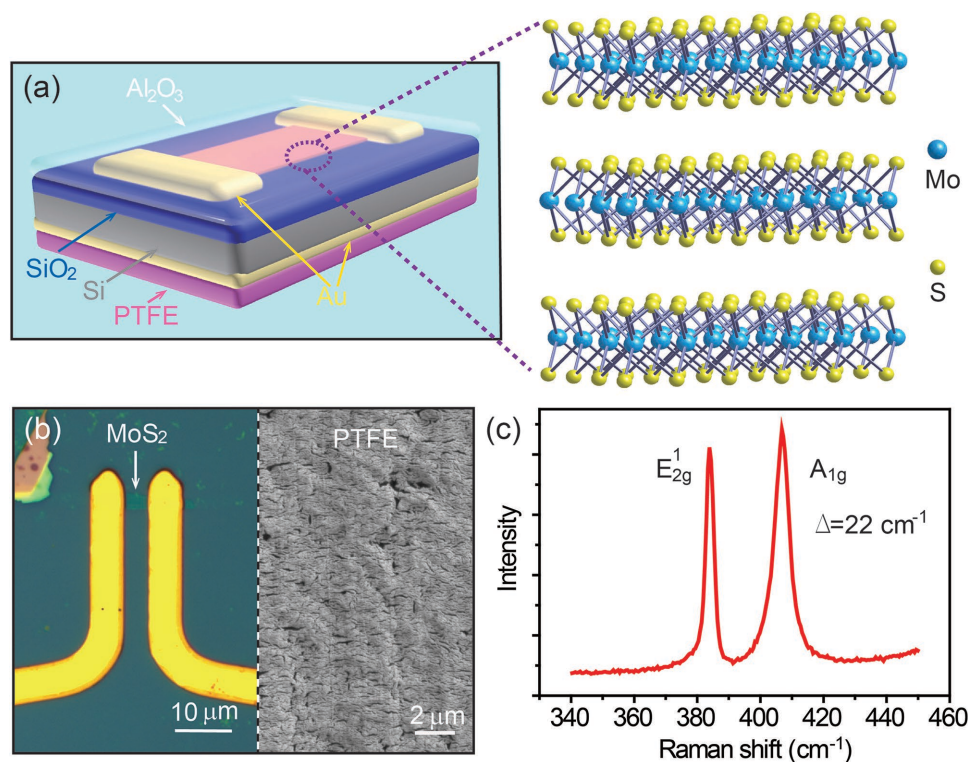


Figure 1. Structure of MoS₂ tribotronic transistor and characterization of MoS₂ flake. a) Schematic illustration of the MoS₂ tribotronic transistor. Inset on the right-hand: side-view of the three-layered MoS₂ crystal structure used in this device. b) Optical graph of the as-fabricated MoS₂ transistor (left hand) and SEM image of the PTFE thin film surface with etched micro/nanostructures (right hand). c) Raman spectrum of the MoS₂ flake for this device.

drain electrodes were precisely patterned on MoS₂ flakes by UV lithography and followed by successively evaporation of Cr and Au. A conductive and charge-induced layer of 50 nm Au (floating gate) was deposited on the bottom surface of the silicon substrate with ohmic contact, underneath which a thin PTFE film with a thickness of 25 μm and an area of $14 \times 14 \text{ mm}^2$ was smoothly attached, serving as a polymer frictional layer of the S-TENG. A 30 nm thick layer of high-quality Al₂O₃ was deposited on the top of the MoS₂ transistor by atomic layer deposition to package the whole device with stability. The optical graph of the device and the scanning electron microscope (SEM) image of the PTFE surface are illustrated in Figure 1b. The conduction channel of the MoS₂ tribotronic transistor is 3 μm in length and 4 μm in width, respectively. Micro/nanostructures of the PTFE surface were etched by the inductively coupled plasma process to enhance the efficiency of contact electrification. Before packaging the device (Al₂O₃ layer), the thickness of the MoS₂ flake was confirmed by Raman spectrum (Figure S1, Supporting information). Figure 1c shows that the in-plane E_{2g}¹ mode and out-of-plane A_{1g} mode is 22 cm⁻¹, indicating that the MoS₂ flake in this device is three layered.^[11,28]

2.2. Principle of the MoS₂ Tribotronic Transistor

The working principle of the MoS₂ tribotronic transistor, based on the coupling effects of contact electrification, electrostatic induction, and field effect, is schematically illustrated

in Figure 2. The structure of the tested device is vertically composed of a MoS₂ based FET, a fixed PTFE layer, and a moving aluminum layer as the other frictional layer of the S-TENG, which is shown in Figure 2a(i). In the initial position (Figure 2a(ii)), the PTFE and aluminum layers are in full contact with each other, resulting in charge transfer between them. According to the triboelectric series, electrons will be injected from the aluminum to PTFE, leaving net positive electrostatic charges on the aluminum layer and net negative electrostatic charges on the PTFE film.^[17,29] At this moment, the produced triboelectric charges with opposite polarities are fully balanced, leading to no influence on the floating gate and the conduction channel width. Once the positively charged aluminum layer vertically separates from the PTFE film at a certain distance (Figure 2a(iii)), part of the negative triboelectric charges on the PTFE film surface will lose the constraint due to the edge electric field leakage from the finite-sized PTFE film and aluminum layer.^[23,29] The unscreened negative charges can give rise to an inner electric field across the grounded source electrode and the gate, which is equivalent to applying a negative voltage on the traditional back gate of a MoS₂ transistor. Thus, some free electrons are depleted in the n-type MoS₂ channel, which will decrease the carrier (electron) density and the corresponding drain-source current. When the moving aluminum layer and PTFE are fully separated at a certain distance (Figure 2a(iv)), the induced inner negative gate voltage reaches its maximum value while the carrier (electron) density in the channel and the drain-source current approaches the minimum.

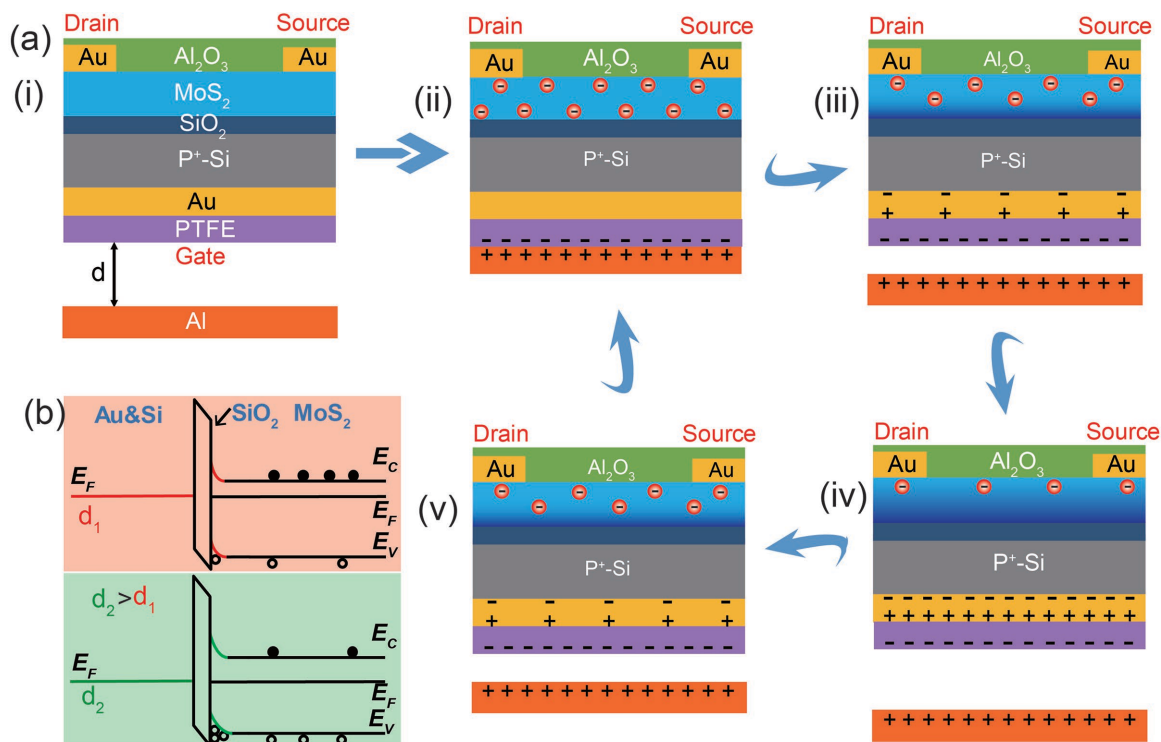


Figure 2. Working principle of the MoS₂ tribotronic transistor. a) Side views of the schematic structure of MoS₂ tribotronic transistor to interpret the change in carrier density with different separation distances. b) Energy band diagram illustrating the metal–insulator–semiconductor capacitor in the device at negative gate voltage. With the increase of separation distance, the induced negative charges on the floating gate increase, resulting in less mobile electrons in the channel; see the text for details.

As the aluminum layer moves backward gradually (Figure 2a(v)), the induced negative gate voltage is decreased, which will increase the carrier density and lead to a rise in the drain-source current. When the aluminum layer and the PTFE thin film come into contact again (Figure 2a(ii)), the negative charges on the PTFE layer are fully balanced again by the positive charges on the moving aluminum layer and has no effects on the MoS₂ channel, which turns the carrier density and the drain-source current back to the initial state. This full cycle of the triboelectric potential generation and gating process on the MoS₂ FET demonstrates that the inner gate voltage can be generated and controlled by the separation distance between the two frictional layers, which has the same effect of applying an external gate voltage. A schematic band diagram is proposed to interpret the stated gating mechanism of the S-TENG on the transistor, as illustrated in Figure 2b. As the separation distance between the two frictional layers increases ($d_2 > d_1$), the triboelectric-charge induced negative potential of the floating gate increases, which will deplete more free electrons and accumulate more holes in the n-type MoS₂ channel and thus decrease the drain-source current.^[30]

2.3. Characteristics of the MoS₂ Transistor with External Voltages

The electrical characterization of the MoS₂ tribotronic transistor was performed on a shielded probe and a semiconductor parameter analyzer (Keithley 4200) at room temperature. Because of the photoelectrical effect of MoS₂, all measurements

were conducted in the dark to avoid the influence of photogenerated current at room temperature. We first characterized the back floating gate (Au) electrically controlled response of the MoS₂ transistor by a bias voltage applied to drain and step voltages to the floating gate with the source grounded. The typical output and transfer characteristics are shown in Figure 3a,b, respectively. The $I_{ds}-V_{ds}$ output characteristics exhibit linear behaviors with different gate voltages, and the $I_{ds}-V_{gs}$ transfer curves at the bias drain voltage of 3 V present I_{ds} increase with the rising gate voltage. The measurement results have validated that the MoS₂ is n-type for the mobile electrons accumulation in the channel with the positive gate voltage^[2] and the on/off ratio of the MoS₂ transistor is about 10³.

2.4. Response of the MoS₂ Tribotronic Transistor

Next, we characterized the response of MoS₂ tribotronic transistor at different separation distances. The MoS₂ tribotronic transistor was fastened on a fixed bracket while the moving aluminum layer was supported by an acrylic plate mounted on a linear motor, providing an effective way to accurately control the separation distance between the two frictional layers. The output responses of the device at different separation distances are systematically interpreted in Figure 4. The distance-dependent output characteristics are presented in Figure 4a under 0 V bias drain voltage. It is observed that the increasing separation distance results in the decreased drain-source

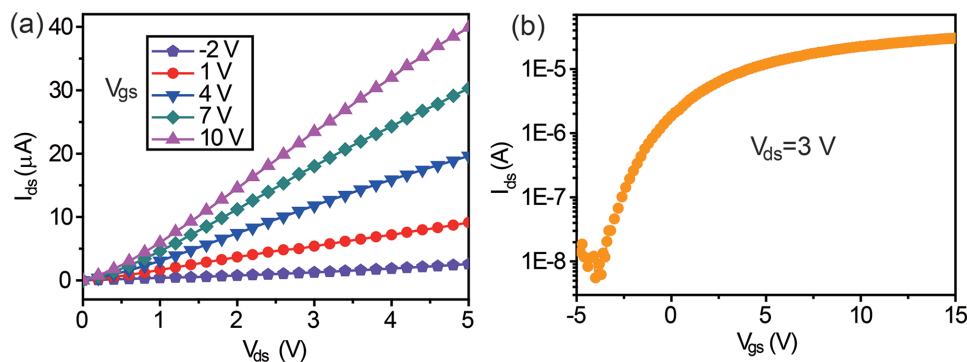


Figure 3. Characterization of the MoS₂ transistor with external voltages applied to the gate. a) Output characteristics I_{ds} – V_{ds} for different V_{gs} . b) Transfer characteristics I_{ds} – V_{gs} with the applied bias voltage V_{ds} of 3 V. The source is always grounded.

current, which is equivalent to applying an externally decreasing step voltage to the floating gate as shown in Figure 3a, and demonstrated that the output voltage of the S-TENG could effectively work as a gate to tune/control charge carrier transport in the transistor. The change and relative change in drain-source current derived from Figure 4a are presented in Figure S2 of the Supporting Information.

Figure 4b shows the drain-source current response at multiseparation-distances with a fixed drain voltage of 1 V. The aluminum layer is driven by the programmed Lin-mot and reciprocating between the origin (x_0 , 40 mm distance from the PTFE

film surface) and the destination (x_1) with a cycle period of ≈ 2.4 s (the left-hand inset in Figure 4b). The separation distance (d) between the aluminum layer and PTFE film in those moving cycle is defined as following: $d = x_0 - x_1$. It can be clearly seen that the drain-source current decreases with the increasing separation distance, indicating that the conduction channel width decreases with the increasing distance, which is consistent with the above analysis shown in Figure 2a. In a single moving cycle of fully contact and entirely separation, the drain-source current can be tuned from 15.74 to 1.56 μA , nearly for ten times change. As displayed in the right-hand inset of Figure 4b, the

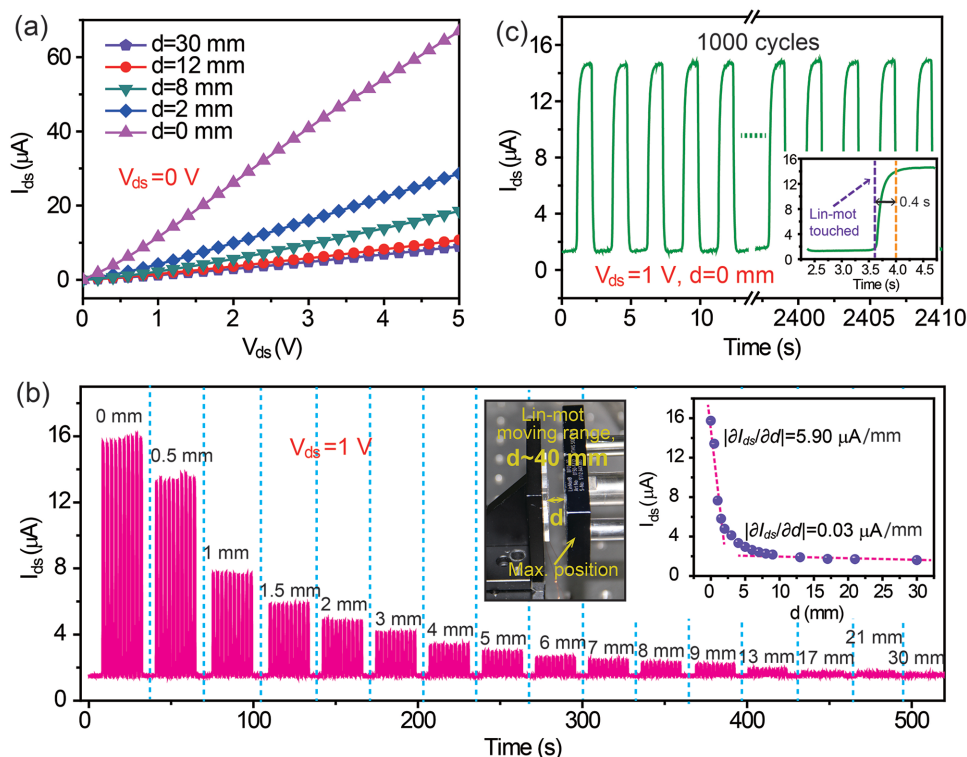


Figure 4. Response of the MoS₂ tribotronic transistor. a) Output characteristics I_{ds} – V_{ds} with the PTFE and aluminum separated at different distances. b) I_{ds} response for different separation distances when $V_{ds} = 1$ V. The left-hand inset: the testing set for the device. The transistor is fastened on a fixed bracket while the moving aluminum layer mounted on a linear motor. The original distance between them is 40 mm. The right-hand inset: I_{ds} is plotted as a function of the separation distance. c) Stability test for the device. I_{ds} shows very little hysteresis and good repeatability after ≈ 1000 cycles. The rising time is about 0.4 s.

drain-source current was plotted as a function of the separation distance, which elucidates that the current first sharply drops and then reaches saturation with the increased separation distance. The change in the drain-source current versus the separation distance can be defined as the slope ($\partial I_{ds}/\partial d$) of the dashed line in the right-hand inset of Figure 4b. In the range of $d < 2$ mm, the device shows $5.90 \mu\text{A}$ sensitive change in drain-source current per millimeter. While in the range of $d > 6$ mm, the change exhibits $0.03 \mu\text{A mm}^{-1}$, nearly 200 times smaller than that of $d < 2$ mm. This decline can be attributed to the decreased change of the induced positive/negative charges in the floating gate (Au) with the increased separation distance. The measurements in thousands of cycles at the separation distance of $d = 0$ and bias drain voltage of 1 V were carried out to validate the stability and repeatability of the device, as shown in Figure 4c and Figure S3 of the Supporting Information. Within 40 min, the drain-source current shows very little hysteresis and can be reproducibly cycled for thousands of times. As the time delay of the Lin-mot controlling system, the rising time between the maximum current value and

the minimum current value as labeled in the inset is about 0.4 s. These results indicate that our device may also work as an accurate and stable displacement sensor, especially in the small range.

2.5. Application of the Device as a Tactile Switch

It is generally believed that electrostatic charges on human fingers can accidentally destroy electronic devices, most notably for complementary metal-oxide-semiconductor (MOS) integrated circuits and MOS FETs. However, a layer of PTFE thin film simply attached to the floating gate of MoS₂ transistor not only protects it from this damage but also functions as an effective gate when a finger touches the device. Here we demonstrate that our MoS₂ tribotronic device can be used as a smart tactile switch, which is directly triggered by finger touch (on) and release (off). In this configuration, the human skin (finger) acts as a frictional layer, instead of the aluminum layer stated above. As reported previously, the human skin is more positive than

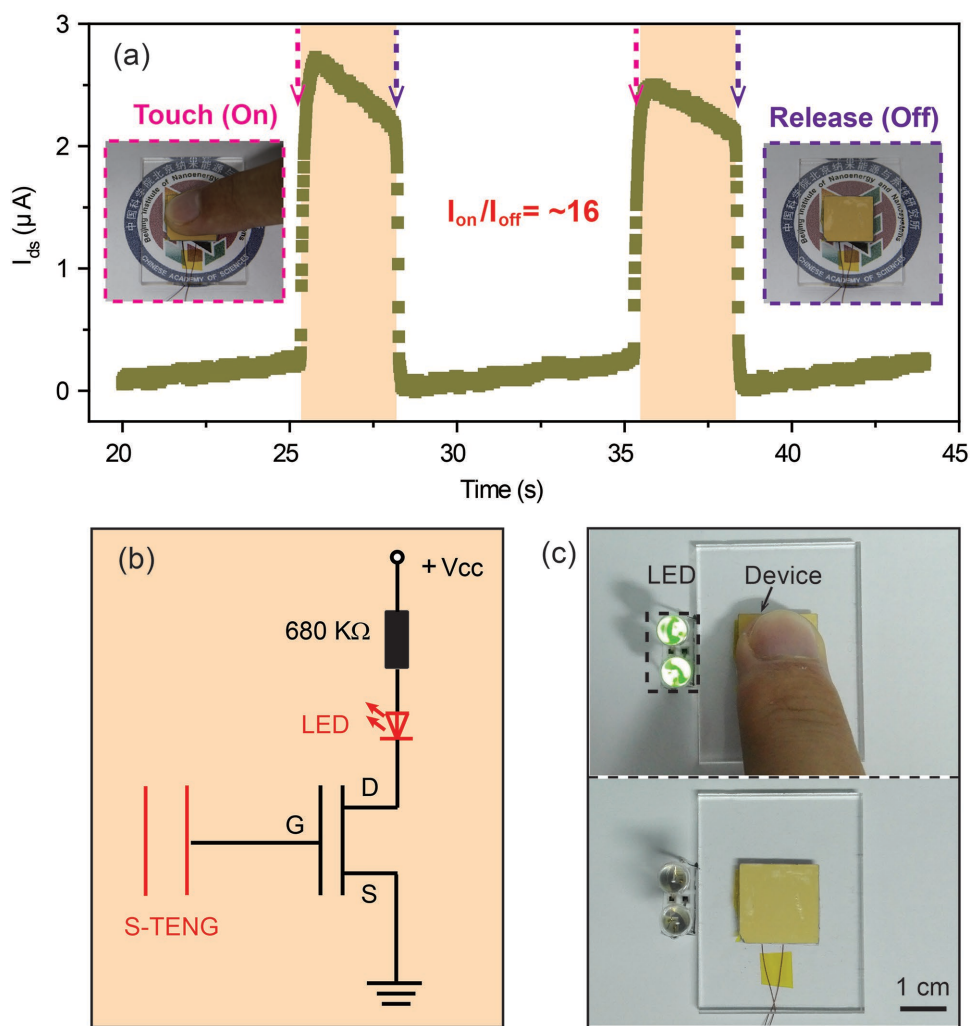


Figure 5. Application of the MoS₂ tribotronic transistor as a finger-triggered active smart tactile switch. a) Finger-triggered response of I_{ds} . The on/off ratio is about ≈ 16 . b) The equivalent electrical circuit of the device. Light-emitting diodes with a current-limiting resistor in series are used to display the on/off state of the smart tactile switch. The bias voltage ($+V_{cc}$) is 0.2 V. c) Photographs showing that two LEDs can be switched on/off directly by the finger touch/release instead of conventional applied gate voltage.

PTFE in the triboelectric series.^[31] When the finger touches the PTFE film, charge transfer happens between them, resulting in the finger with positive electrostatic charges and the PTFE film with negative electrostatic charges. At this moment, the negative charges on the surface of PTFE are balanced by the positive charges on the skin and the induced negative charges on the upper surface of the floating gate decreased. Therefore, the negative electric potential of the floating gate can be increased to enhance the electron density of MoS₂ conduction channel and thus the drain-source current, as shown in Figure 5a. The finger-triggered on/off ratio can be as high as 16, which is higher than the case with the aluminum plate. It is possibly because that much more charge transfer happens between the human skin and the PTFE film. The equivalent electrical circuit of the MoS₂ tribotronic transistor based on S-TENG for the application in active smart tactile switch is illustrated in Figure 5b. Two light-emitting diodes (LEDs) with a current-limiting resistor in series are used to display the on/off state of the switch. The demo optical graphs are shown in Figure 5c, which presents that the two LEDs are switched on with a finger touching the frictional layer (PTFE film) of the MoS₂ tribotronic transistor, while switched off without finger touch.

3. Conclusion

In conclusion, we have demonstrated an MoS₂ tribotronic transistor based on S-TENG and MoS₂ FETs with a frictional layer of PTFE film on the floating gate. With the coupling effects of triboelectrification and electrostatic induction, the inner gate voltage can be produced by the metal friction layer and used for tuning the charge carrier transport in the MoS₂ conduction channel in place of the traditional external gate voltage. Moreover, the device is used as an active smart tactile switch triggered by a human finger, in which the on/off ratio is as high as 16. This MoS₂ tribotronic transistor can also be widely applied as displacement sensors, visualized touch sensors, and smart skin. This work has extended the emerging tribotronics to 2D materials and demonstrated the new field may have innovative and important potential applications in the fields of wearable healthcare, human-computer interfacing, and artificial intelligence.

Supporting Information

Supporting Information is available from the Wiley Online Library or from the author.

Acknowledgements

F.X. and L.C. contributed equally to this work. The authors thank Dr. Tao Jiang for helpful discussions. Research was supported by the Hightower Chair foundation, and the “thousands talents” program for pioneer researcher and his innovation team, China, National Natural Science Foundation of China (Grant Nos. 51432005 and 51475099), and U.S. Department of Energy, Office of Basic Energy Sciences (Award DE-FG02-07ER46394).

Received: October 19, 2015
Revised: December 31, 2015
Published online:

- [1] B. Radisavljevic, A. Radenovic, J. Brivio, V. Giacometti, A. Kis, *Nat. Nanotech.* **2011**, *6*, 147.
- [2] S. Kim, A. Konar, W. S. Hwang, J. H. Lee, J. Lee, J. Yang, C. Jung, H. Kim, J. B. Yoo, J. Y. Choi, Y. W. Jin, S. Y. Lee, D. Jena, W. Choi, K. Kim, *Nat. Commun.* **2012**, *3*, 1011.
- [3] H. Li, Z. Yin, Q. He, H. Li, X. Huang, G. Lu, D. W. Fam, A. I. Tok, Q. Zhang, H. Zhang, *Small* **2012**, *8*, 63.
- [4] Z. Y. Yin, H. Li, H. Li, L. Jiang, Y. M. Shi, Y. H. Sun, G. Lu, Q. Zhang, X. D. Chen, H. Zhang, *ACS Nano* **2012**, *6*, 74.
- [5] O. Lopez-Sanchez, D. Lembke, M. Kayci, A. Radenovic, A. Kis, *Nat. Nanotech.* **2013**, *8*, 497.
- [6] H. Li, J. Wu, Z. Yin, H. Zhang, *Acc. Chem. Res.* **2014**, *47*, 1067.
- [7] K.-A. N. Duerloo, M. T. Ong, E. J. Reed, *J. Phys. Chem. Lett.* **2012**, *3*, 2871.
- [8] W. Z. Wu, L. Wang, Y. Li, F. Zhang, L. Lin, S. M. Niu, D. Chenet, X. Zhang, Y. Hao, T. F. Heinz, J. Hone, Z. L. Wang, *Nature* **2014**, *514*, 470.
- [9] H. Zhu, Y. Wang, J. Xiao, M. Liu, S. Xiong, Z. J. Wong, Z. Ye, Y. Ye, X. Yin, X. Zhang, *Nat. Nanotech.* **2015**, *10*, 151.
- [10] J. Qi, Y. W. Lan, A. Z. Stieg, J. H. Chen, Y. L. Zhong, L. J. Li, C. D. Chen, Y. Zhang, K. L. Wang, *Nat. Commun.* **2015**, *6*, 7430.
- [11] R. Ganatra, Q. Zhang, *ACS Nano* **2014**, *8*, 4074.
- [12] K. F. Mak, C. Lee, J. Hone, J. Shan, T. F. Heinz, *Phys. Rev. Lett.* **2010**, *105*, 136805.
- [13] J. K. Ellis, M. J. Lucero, G. E. Scuseria, *Appl. Phys. Lett.* **2011**, *99*, 261908.
- [14] R. Cheng, S. Jiang, Y. Chen, Y. Liu, N. Weiss, H. C. Cheng, H. Wu, Y. Huang, X. F. Duan, *Nat. Commun.* **2014**, *5*, 5143.
- [15] W. Park, J. Yang, C. Kang, Y. Lee, H. Hwang, C. Cho, S. Lim, S. Kang, W. Hong, S. Lee, S. Lee, B. Lee, *Nanotechnology* **2013**, *24*, 475501.
- [16] L. Chen, F. Xue, X. Li, X. Huang, L. Wang, J. Kou, Z. L. Wang, *ACS Nano*, DOI: 10.1021/acs.nano.5b07121.
- [17] F. Fan, Q. Tian, Z. L. Wang, *Nano Energy* **2012**, *1*, 328.
- [18] Z. L. Wang, *ACS Nano* **2013**, *7*, 9533.
- [19] C. Zhang, T. Zhou, W. Tang, C. Han, L. Zhang, Z. L. Wang, *Adv. Energy Mater.* **2014**, *4*, 1301798.
- [20] G. Zhu, J. Chen, T. Zhang, Q. Jing, Z. L. Wang, *Nat. Commun.* **2014**, *5*, 3426.
- [21] G. Zhu, Y. Zhou, P. Bai, X. Meng, Q. Jing, J. Chen, Z. L. Wang, *Adv. Mater.* **2014**, *26*, 3788.
- [22] J. Luo, F. Fan, T. Zhou, W. Tang, F. Xue, Z. L. Wang, *Extreme Mech. Lett.* **2015**, *2*, 28.
- [23] C. Zhang, W. Tang, L. Zhang, C. Han, Z. L. Wang, *ACS Nano* **2014**, *8*, 8702.
- [24] C. Zhang, L. Zhang, W. Tang, C. Han, Z. L. Wang, *Adv. Mater.* **2015**, *27*, 3533.
- [25] C. Zhang, J. Li, C. Han, L. Zhang, X. Chen, L. Wang, G. Dong, Z. L. Wang, *Adv. Funct. Mater.* **2015**, *25*, 5625.
- [26] J. Li, C. Zhang, L. Duan, L. Zhang, L. Wang, G. Dong, Z. L. Wang, *Adv. Mater.* **2016**, *28*, 106.
- [27] C. Zhang, Z. H. Zhang, X. Yang, T. Zhou, C. B. Han, Z. L. Wang, *Adv. Funct. Mater.* **2015**, DOI: 10.1002/adfm.201504919.
- [28] B. Liu, L. Chen, G. Liu, A. Abbas, M. Fathi, C. Zhou, *ACS Nano* **2014**, *8*, 5304.
- [29] Y. Yang, Y. Zhou, H. Zhang, Y. Liu, S. Lee, Z. L. Wang, *Adv. Mater.* **2013**, *25*, 6594.
- [30] S. M. Size, K. K. Ng, *Physics of Semiconductor Devices*, John Wiley & Sons, New York, NY, USA **1981**.
- [31] J. Lee, R. Hinchet, T. Kim, H. Ryu, W. Seung, H. Yoon, S. Kim, *Adv. Mater.* **2015**, *27*, 5553.